

PCCP

Accepted Manuscript



This is an *Accepted Manuscript*, which has been through the Royal Society of Chemistry peer review process and has been accepted for publication.

Accepted Manuscripts are published online shortly after acceptance, before technical editing, formatting and proof reading. Using this free service, authors can make their results available to the community, in citable form, before we publish the edited article. We will replace this *Accepted Manuscript* with the edited and formatted *Advance Article* as soon as it is available.

You can find more information about *Accepted Manuscripts* in the [Information for Authors](#).

Please note that technical editing may introduce minor changes to the text and/or graphics, which may alter content. The journal's standard [Terms & Conditions](#) and the [Ethical guidelines](#) still apply. In no event shall the Royal Society of Chemistry be held responsible for any errors or omissions in this *Accepted Manuscript* or any consequences arising from the use of any information it contains.

Remarkably improving microwave absorption by cloaking micro-scaled tetrapod hollow with helical carbon nanofibers

Cite this: DOI: 10.1039/x0xx00000x

Xian Jian,^{a,b} Xiangnan Chen,^b Zuowan Zhou,^{*b} Gang Li,^c Man Jiang,^b Xiaoling Xu,^b Jun Lu,^b Qiming Li,^d Yong Wang,^b Jihua Gou^e and David Hui^f

Received 00th January 2014,
Accepted 00th January 2014

DOI: 10.1039/x0xx00000x

www.rsc.org/

Helical nanofibers are prepared through an in-situ growth on the surface of tetrapod-shaped ZnO whisker (T-ZnO), by employing precursor decomposition method and adding substrate. After heat treatment at 900 °C under argon, this new composite material, named helical nanofiber/T-ZnO, undergoes a significant change in the morphology and structure. The T-ZnO transforms from solid tetrapod ZnO to micro-scaled tetrapod hollow carbon film by reduction of the organic fiber at 900 °C. Besides, helical carbon nanofibers generate from the carbonization of helical nanofibers, maintaining the helical morphology. Interestingly, HCNFs with T-hollow exhibit remarkably improvement in electromagnetic wave loss compared with the pure helical nanofibers. The enhanced loss ability may arise from the efficient dielectric friction, interface effect in the complex nanostructures and the micro-scaled tetrapod-hollow structure.

^a School of Energy Science and Engineering, University of Electronic Science and Technology of China, Chengdu, Sichuan 611731, China. Email: jianxian20033835@163.com or jianxian@uestc.edu.cn

^b Key Laboratory of Advanced Technologies of Materials (Ministry of Education), School of Materials Science and Engineering, Southwest Jiaotong University, Chengdu 610031, China. Fax, Tel: +86 028-87600454. E-mail: zwzhou@at-c.net (Z. Zhou).

^c Research Center for Eco-Environmental Sciences, Chinese Academy of Sciences, Beijing 100085, China. Email: gangli@rcees.ac.cn

^d Shanghai Institute of Applied Physics, Key Laboratory of Nuclear Radiation and Nuclear Energy Technology Chinese Academy of Sciences, Shanghai 201800, China

^e Department of Mechanical, Materials and Aerospace Engineering, University of Central Florida, Orlando, FL 32816, United States

^f Department of Mechanical Engineering, University of New Orleans, New Orleans, LA 70148, United States

Introduction

Advances in catalysis are critical to modern nanotechnology.^{1, 2} At present, nanocatalyst has shown promising application potentials in many fields. They can be used in a wide variety of applications such as synthesis,³ electronics^{4, 5} and medicine.⁶ Carrier-supported catalyst is a simple and effective method to enhance or alter the catalytic performance.^{2, 7-10} Combined with appropriate interaction of substrate, catalysts with designed functions are realized. For example, both pure Cu and ZnO don't possess good catalytic property during the methanol synthesis using gas mixtures of $H_2/CO_2/CO$. However, $Cu/ZnO/Al_2O_3$ is a high-performance industrial catalyst for the existence of active site consisting of Cu decorated with Zn atoms.¹¹ Besides, the introduction of substrate helps form some catalysts with high uniformity and selectivity. Ren *et al.* reported helical carbon nanofibers (HCNFs) synthesized by the catalytic decomposition of acetylene using supported copper catalysts including Cu/SiO_2 , Cu/TiO_2 , Cu/Al_2O_3 and Cu/MgO particles.¹² And Ren *et al.* found that the content of HCNFs strongly depended on the types of catalytic supports and ratios of Cu/support.¹² At present, preparing helical nanofibers¹³⁻¹⁶ such as HCNFs using novel catalyst has attracted researchers' great interests in the field of synthesis and related nanomaterials.¹⁷⁻¹⁹ However, few literature concerns the interaction between ZnO matrix and Cu nanocrystal in helical fibers synthesis, which may induce great influence on the catalyst property.

In the field of microwave absorption, carbon-based composite materials have some advantages compared with traditional ferrite materials, such as low density and high values of complex permittivity, which may improve the microwave absorption property and electromagnetic interference shielding effect.²⁰ In fact, microwave absorption property is influenced by the interfacial interactions of novel structure. Bi *et al.* reported that the decoration of bowl-like hollow Fe_3O_4 spheres on both sides of the r-GO nanosheets greatly enhance the dielectric loss of the materials, resulting in a wider absorption band and a larger reflection loss in frequency range of 2–18 GHz.²¹ The pore in the micro-spheres also increases the microwave loss of specimens due to spin-transfer

effects.²² So it is valuable to design novel structures with multi-scale or different morphology such as grain size, porosity and intra- or inter-granular pores, etc.

Previous study found that coordination polymerization of acetylene occurs on the surface of Cu nanocrystal²³, and the helical or straight carbon fiber can be selectively prepared using a gas-induced technique.^{24, 25} Here, we find that the interaction between Cu and ZnO crystal is fairly strong and has substantial impact during the catalysis of acetylene by copper. By adjusting the molar concentration of copper, we can selectively obtain a corn-like ZnO or helical fiber/T-ZnO. In addition, a novel multiple structures named helical carbon fibers with tetrapod-hollow feature (mentioned as "T-hollow" hereafter) are prepared from the carbonization of helical fiber/T-ZnO material after thermal treatment. Compared with high-purity helical nanofiber, T-hollow exhibits excellent microwave absorption properties.

Results and discussion

Preparation of helical nanofibers/T-ZnO

The process of preparing helical nanofibers/T-ZnO is depicted in **Fig. 1**. T-ZnO whiskers with a diameter of 20 μm were used as a catalyst substrate. The obtained supported catalyst, namely copper tartrate/T-ZnO, is used for the growth of helical nanofibers according to our earlier reported gas-induced method under C_2H_2 at 271°C.²⁵

The amount of catalyst precursors loaded on the T-ZnO substrate significantly affects the size of the Cu nanocrystals and the degree of their agglomeration. **Fig. 2** shows electron microscopic images of copper tartrate/T-ZnO (**Fig. 2a, b**) and Cu/T-ZnO (**Fig. 2c, d**) with Cu concentration of 0.6 mol%. The SEM results show that copper tartrate uniformly adheres to the surface of T-ZnO and decomposes into Cu nanocrystals under H_2 at 271 °C. Driven by the minimization of their surface energy, Cu nanocrystals aggregate as shown in **Fig. 2d**. However, the proper size of those Cu nanocrystals facilitates the preparation of original helical nanofibers according to our previous study.^{24, 25} Furthermore, the Cu nanocrystals become smaller and

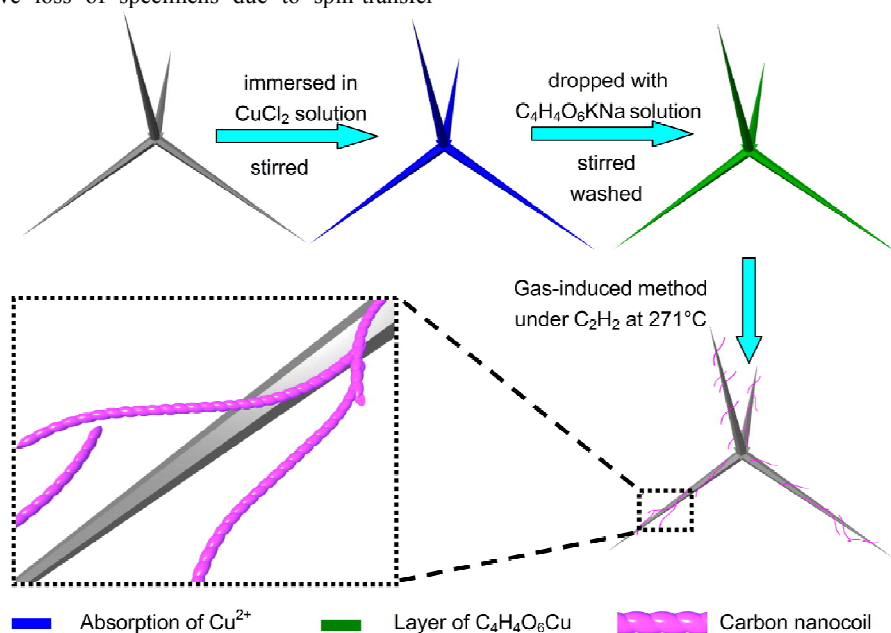


Fig. 1 Scheme for the preparation of original helical nanofibers on the surface of T-ZnO.

firmly intersperses on the surface of T-ZnO by decreasing the Cu constituent to 0.2~0.4 mol%, as shown in Fig. S1a, b (see Supporting Information). Contrarily, the as-prepared Cu particles become more varied and tend to aggregate in case of the Cu content increasing up to 0.8 mol% or 1.0 mol% (see Fig. S1 d, e). Then the size and uniformity of Cu particles mainly depend strongly on the feeding molar concentration of copper tartrate.

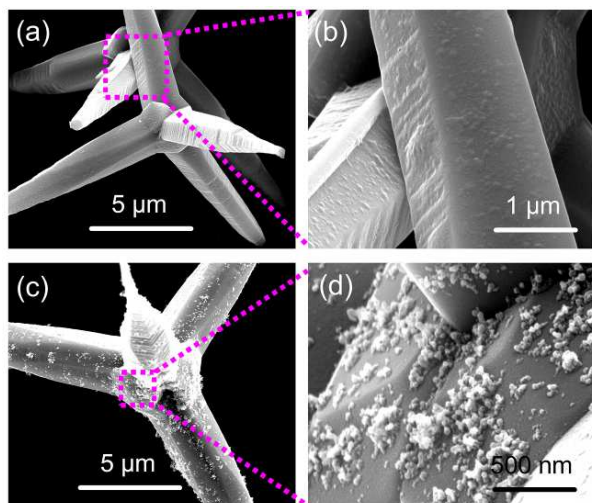


Fig. 2 SEM images of (a, b) copper tartrate/T-ZnO and (c, d) Cu/T-ZnO (Cu/ZnO=0.6 mol%).

Structural analysis of helical nanofibers/T-ZnO

Though copper tartrate decomposes into Cu nanocrystals and some gaseous reaction products above 250 °C,²⁶ it is unclear whether these Cu nanocrystals remain on the surface of T-ZnO during the decomposition process. We herein investigate the Cu/T-ZnO products by X-ray powder diffraction (XRD) and X-ray photoelectron spectroscopy (XPS). XRD patterns of the Cu/T-ZnO composites are shown in Fig. 3, together with pure T-ZnO materials as compared. It is intriguing that there is not Cu phase appearing in the obtained Cu/T-ZnO products. The XRD results are inconsistent to the SEM observation (see Supplementary Material, Fig. S1), indicating that Cu particles lie on the T-ZnO surface. The reason may be that the Cu concentration is too low to go beyond XRD detection limit. As the Cu constituent increases, the diffraction peak of Cu phase is detected at 43.3° corresponding to the Cu (111), as presented in Fig. S2.

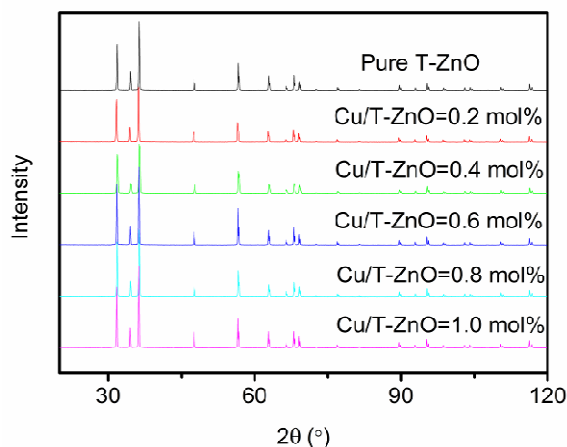


Fig. 3 XRD patterns of pure T-ZnO and Cu/T-ZnO at the range of 0.2 ~1.0 mol%.

XRD and XPS analyses have been used to identify the constituent and the valence state of the samples. The XPS spectra of Cu/T-ZnO (0.4 mol%) are shown in Fig. 4 and Fig. S3, which indicates that Cu, Zn and O elements exist in the products. The Cu 2p_{3/2} binding energy in Cu/T-ZnO sample is 933.5 eV. As the Cu 2p_{3/2} binding energies for Cu,²⁷ Cu₂O²⁸ and CuO^{29,30} are 932.6, 932.55 and 934.6 eV, respectively. The satellite peak appears in the high-resolution XPS shown in Fig. 4(a), which is the typical feature of copper oxides. Then these nanocrystals on the surface of T-ZnO are identified to be CuO possibly due to the strong interaction of T-ZnO. Similarly, as shown in Fig. 4(b), we find that the binding energies for Zn 2p_{3/2} and Zn 2p_{1/2} are 1022.4 and 1045.5 eV, respectively. The values are larger than those reported by Jing *et al.*³¹, from which we can further suggest the formation of Cu⁺-O-Zn⁺⁺ hybridization structure on the surface of T-ZnO. It is possible that Cu is easily oxidized in air. However, CuO tends to favor the growth of straight nanofibers, which has been proposed by the previous study.³²

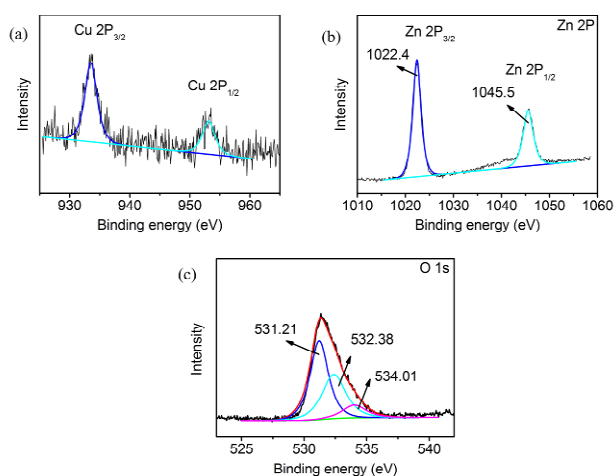


Fig. 4 XPS spectra of Cu/T-ZnO: (a) Cu 2p, (b) Zn 2p and (c) O 1s.

At relatively low reaction temperature below 300 °C, copper is a type of effective catalyst for synthesis of helical nanofibers.²⁵ Copper nanocrystals disperse well on the surfaces of T-ZnO with copper content being adjusted ranging 0.2~0.4 mol %. The Cu/T-ZnO composite catalyst is effective to *in-situ* synthesize uniform helical nanofiber adhering to the surface of T-ZnO. However, the obtained products don't contain any fibers but a kind of corn stick structure, as shown in Fig. S4. This sample is named corn cob-like T-ZnO. The corn-kernel's sizes are at the range of 32~124 nm and 55~214 nm when molar ratios of Cu/T-ZnO are 0.2 mol% and 0.4 mol%, respectively. As reported in previous paper, CuO is a catalyst for straight carbon nanofibers.³² Then CuO has the ability to promote the polymerization of acetylene forming "corn kernel" fixed on the surface of T-ZnO.

Another extremely, as Cu constituent in the composite catalyst increases to more than 0.8 mol%, fibers generate around the T-ZnO particles as shown in Fig. S5. The fiber diameter becomes larger and its morphology differs from each other. After coordination polymerization of C₂H₂ at 271 °C using Cu/T-ZnO catalyst, three kinds of fibers, including straight nanofiber, nano-helix and micro-helix, exist among the fiber/T-ZnO samples. The formation of mixed-type fiber is due to Cu particles with great diversity in terms of size and shape.

Formation of helical nanofibers/T-ZnO

Several different types of catalysts can lead to the growth of helical carbon fibers.^{33, 34} To obtain high-purity helical nanofibers, the uniform Cu catalyst is essential, since that the morphology of this kind of nanofiber is related to the polygonal nature of Cu particles.^{25, 35} By optimizing the content of Cu, we obtain high-purity helical nanofibers around the T-ZnO particles. Firstly, the molal ratio of Cu to T-ZnO is controlled to be ~ 0.6 mol%. Then, Cu nanocrystals are prepared from the decomposition of copper tetratrate under the effect of acetylene-induction. Finally, high-purity helical nanofibers are *in-situ* synthesized from acetylene polymerization around T-ZnO particles as shown in Fig. 5a and b. Interestingly, a kind of material with novel structure is obtained from the helical nanofibers/T-ZnO composites after heat treatment at 900 °C under Ar for 4 h.

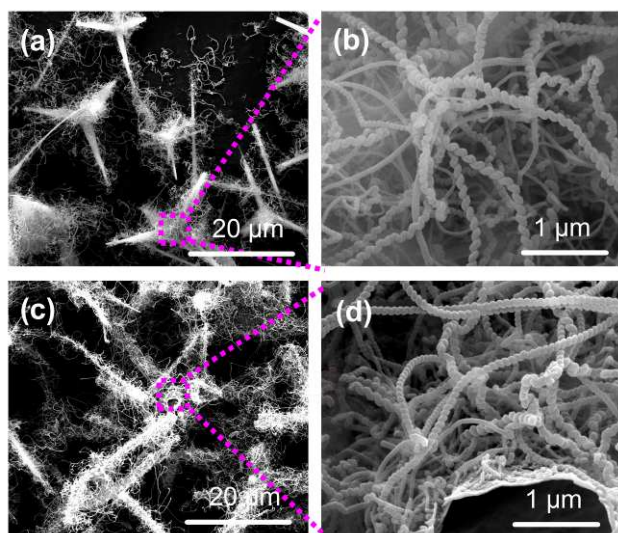


Fig. 5 SEM images of high-purity helical nanofibers/T-ZnO (a, b) using the Cu/T-ZnO (0.6 mol%) as catalyst and helical fiber with tetrapod-hollow (c, d) obtained from the helical nanofibers/T-ZnO composites after heat treatment at 900 °C under Ar for 4 h.

The morphology of this material, named helical fiber with tetrapod-hollow, is shown in Fig. 5c, d. The helical structure of the original helix remains well during the carbonization process. Interestingly, T-ZnO crystals disappear, which brings about tetrapod-hollow structure at the scale range of 1-3 μm. Among the possible causes, we speculate that ZnO is reduced by H₂ or CO releasing from the pyrolysis of helical fibers containing -CH=CH- group.²⁴ Then T-ZnO is transformed from the solid semiconductor into Zn vapor at high temperature of 900 °C. Under the impetus of argon flow, zinc vapor discharges out of the solid sample and assemble together inside of the quartz tube tail, resulting in forming hollow structure. The inference is in agreement with the fact that a black buck having metal luster coheres at the end of the quartz tube. EDX result also verifies the black buck containing Zn and C elements (see Fig. S6). As a result, T-hollow with tetrapod-hollow and multi-scaled porous structures are obtained using such process of heat-treatment.

The morphology and microstructure of the samples are further analyzed in TEM, which reveals that high-purity helical nanofibers are still around T-ZnO particles as shown in Fig. 6a. Helical fibers of the bright-dark contrasts and black T-ZnO pods are observed in the magnified TEM image of Fig. 6b, revealing that helical fibers are amorphous and the pods are of crystalline character. For the carbonized products, a micro-sized hollow structure is observed in the TEM image at a low magnification in Fig. 6c, revealing that T-ZnO has been disappeared after heat-treatment. Moreover, the

helical structure of this nanofiber maintains well as shown in Fig. 6d. Then T-hollow are obtained and they become quasi-graphite from the analysis of the high-magnification TEM image in Fig. 6e. Besides, the TEM results demonstrate the wall of “T-hollow” are amorphous carbon as shown in Fig. S7. XRD patterns of the three samples, namely T-ZnO, helical fibers/T-ZnO and helical fibers with tetrapod-hollow structures are shown in Fig. S8. For the helical fiber/T-ZnO composite, crystalline diffraction peaks of ZnO appear in corresponding XRD patterns, which is mainly because of the amorphous structure for helical fibers and the large mass ratio of the crystalline ZnO. In addition, the XRD result of helical fiber with tetrapod-hollow shows that both quasi-graphite and Cu catalyst remains in this hollow product after heat treatment. The diffraction peaks of ZnO are not detected out, which is strongly re-confirmed that T-ZnO is reduced into metallic Zn vapor, and the Zn vapor escaped from the reaction tube by the carrying gas of argon, resulting in tetrapod-hollow structures creating subsequently.

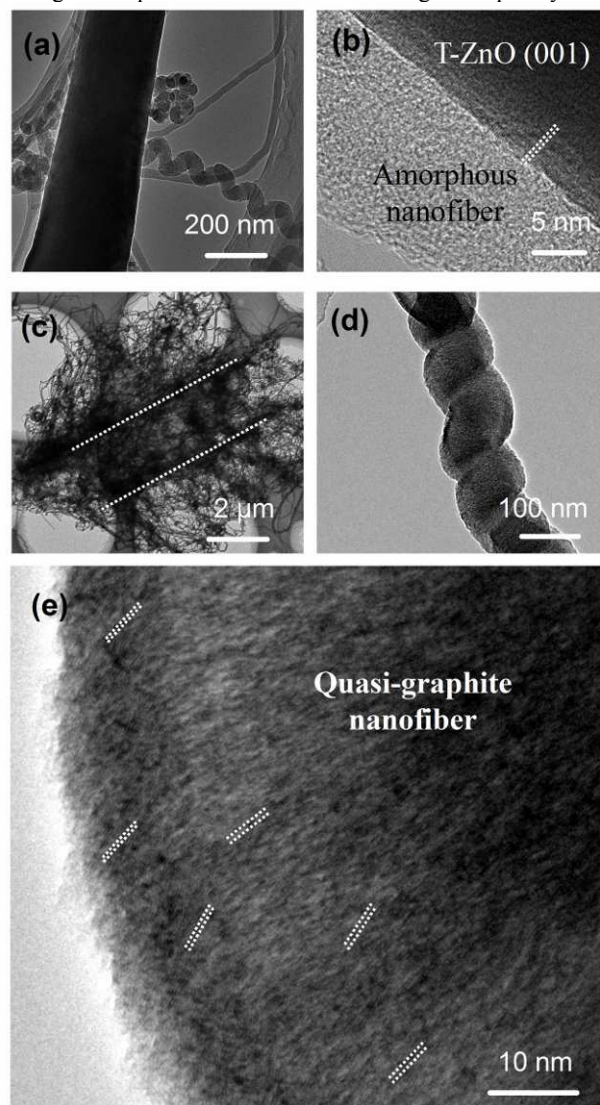


Fig. 6 TEM images of high-purity helical nanofibers/T-ZnO (a, b) using the Cu/T-ZnO (0.6 mol%) as catalyst and helical fiber with tetrapod-hollow (c, d, e) obtained from the helical nanofibers/T-ZnO composites after heat treatment at 900 °C under Ar for 4 h.

Microwave absorption properties of related helical materials

We herein studied the electromagnetic properties of original helical nanofiber, HCNFs and T-hollow across 2–18 GHz frequency ranges. For the three kinds of helical materials, Fig. 7 shows their complex permittivity and permeability consisting of the real part (ϵ' , μ') and imaginary part (ϵ'' , μ'') over the 2–18 GHz range. Both HCNFs and T-hollow have a frequency dependence of complex permittivity, while original helical nanofiber is almost constant at 2–18 GHz. The differences of dielectric characteristics among them are consequences of their intrinsic dielectric loss of proper conductive

objects. The electrical conductivities of HCNFs and T-hollow are about 10^{-1} S/cm measured by four-point probe method, higher than the value ($\sim 10^{-9}$ S/cm) of original helical nanofibers. The electronic conductivity of microwaves absorbent is the key in the microwave application, and should be controlled at an optimum range of 10^{-1} – 10^2 S/cm for microwave penetration into the bulk absorbent.³⁶ Due to the absence of magnetic substance in samples, the helical materials don't exhibit any magnetic behavior, as shown in Fig. 8.

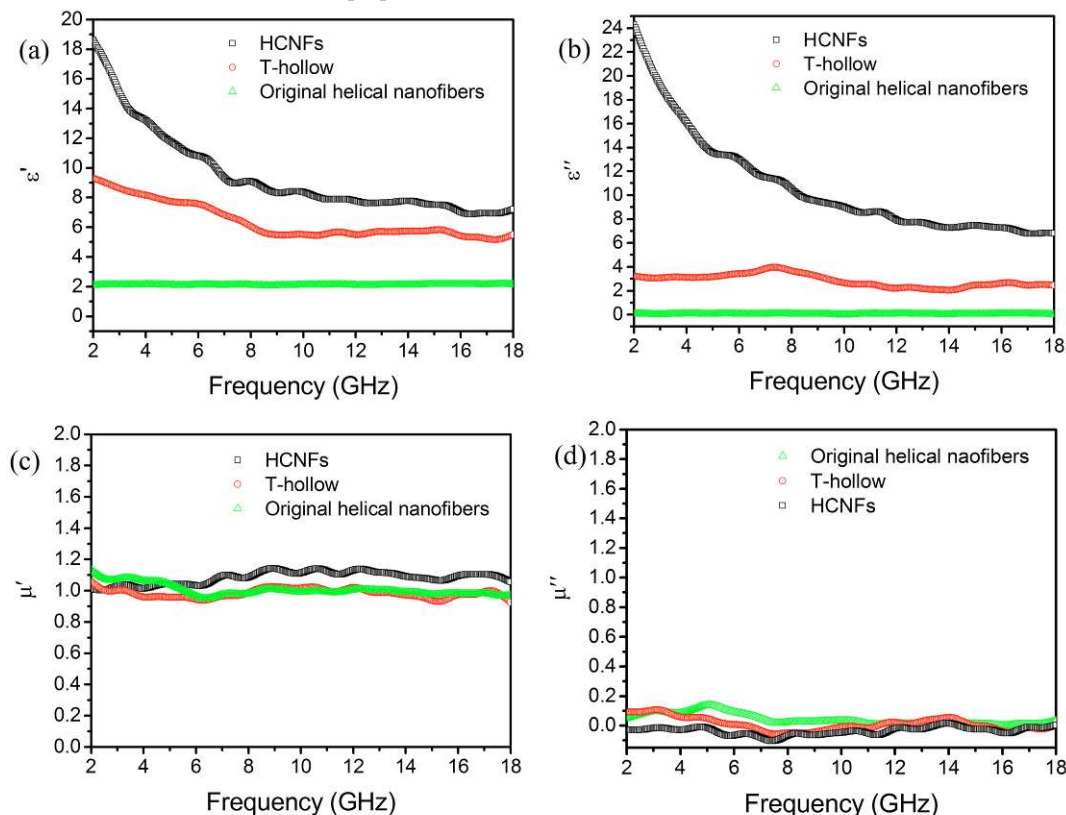


Fig. 7 Measured relative (a, b) complex permittivity and (c, d) complex permeability values of original helical nanofibers, helical carbon nanofibers and helical fiber with tetrapod-hollow. All the measured samples are uniformly mixed with the same weight of wax paraffin (sample:wax = 1:9).

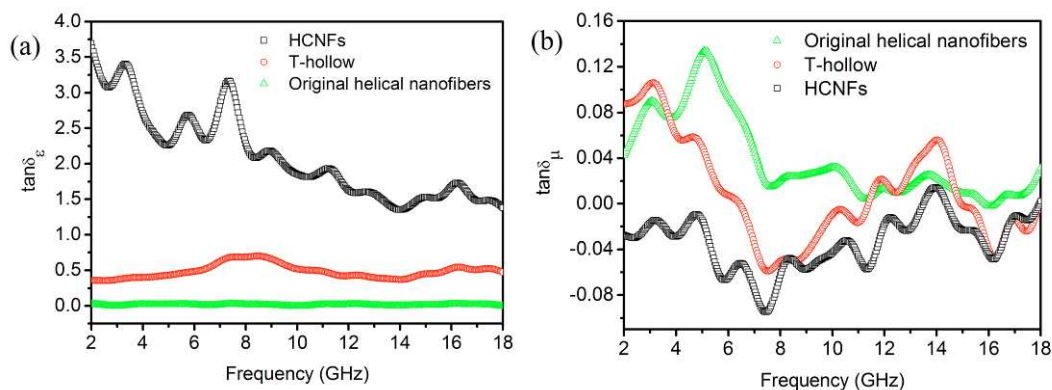


Fig. 8 Measured dielectric and magnetic loss of original helical nanofibers, HCNFs and T-hollow.

Based on the measured data of complex permittivity and permeability, the values of the reflection loss (RL) of original helical nanofiber, HCNFs and T-hollow were calculated according to the

transmit-line theory. Then the microwave absorption properties were estimated using the RL(dB), described as following expression.³⁷

$$RL(dB) = 20 \log \left| \frac{Z_{in} - 1}{Z_{in} + 1} \right| \quad (1)$$

where Z_{in} is the input characteristic impedance at the interface between absorber and air, which can be expressed as

$$Z_{in} = \sqrt{\frac{\mu_r}{\epsilon_r}} \tanh i \frac{2\pi f}{c} \sqrt{\mu_r \epsilon_r} d \quad (2)$$

where the μ_r and ϵ_r are respectively the relative complex permittivity and permeability of absorber, f is the frequency of the electromagnetic wave, c is the velocity of light, and d is the thickness of the absorber.

Fig. 9a shows a comparison of the calculated RL curves over 2–18 GHz frequency range for the samples/wax composites with a thickness of 3 mm. It can be seen that the microwave absorption properties of original helical nanofibers are expected mainly from dielectric loss, with RL values more than -2.0 dB. Compared to the pristine helical nanofibers, the RL performances toward EM waves of carbonized HCNFs are enhanced substantially. The minimum RL of HCNFs and T-hollow are -9.50 and -15.97 dB at 12.3 and 17.7 GHz, respectively as shown in **Fig. 9**. In addition, the frequency related to minimum RL can be modulated by increasing the thickness of absorbers, and the absorption peaks shift to lower frequency accompanied by broadening at effective absorbing frequency bands. As Qin *et al* reported, materials with RL values of less than -10 dB absorption are considered to be suitable EM wave absorbers.³⁸ Then the original helical nanofibers and HCNFs are not good EM wave absorbers, while the introduction of the tetrapod-hollow into the helical fibers is an effective way for compromising the electromagnetic wave loss. Besides, the composite method is another effective way to improve microwave absorption properties.³⁹ The combination of the two approaches might be a potential researching design in the field of EM wave absorbers.

In addition, compared with the original helical nanofiber and HCNFs, we have studied the RL performance of straight fibers including straight original nanofibers and straight carbon fibers. For

straight original fiber without any treatment, the RL values are greater than -2.0 dB, which is similar to the original helical fibers, exhibiting poor behavior of the electromagnetic losses. Owing to their chemical structures, both helical and straight original nanofibers are insulator with electrical conductivities about 10^{-9} S/cm, which goes beyond the suitable range of 10^{-1} – 10^2 S/cm.³⁶ Moreover, one can find that the RL performance of the carbonized straight fibers is improved and the RL values significantly increase compared to the original straight nanofibers as shown in **Fig. 10**. This confirms that carbonization process is effective for actualizing impedance matching by adjusting the electrical conductivity. Besides, both helical and straight carbon nanofibers represent a contiguous level of the electromagnetic losses, suggesting that the helical structure cannot improve the electromagnetic wave loss either.

In the frequency of 2–18 GHz, HCNFs had only dielectric loss and the reflection loss values were higher than -10 dB, while the original helical fibers exhibited neither dielectric loss nor magnetic loss due to the low electrical conductivity. Interestingly, HCNFs with T-hollow exhibited remarkably improvement in electromagnetic wave loss compared with the pure helical nanofibers. The possible reasons for their excellent absorbing properties: (a) A factor responsible for this improvement was identified as an improved impedance match with the increase of conductivity after the carbonization process. (b) Another factor is that more energy may be dissipated due to the hollow structure. Then spin-transfer effects may exist due to the interlayer exchange coupling.²² (c) HCNFs around the hollow structure are composed of many small graphene sheets or carbon clusters like amorphous carbon nanotubes, which exhibit the features of short-range order and long-range disorder. The special features favor the higher performance of electromagnetic wave absorbing property.⁴⁰ (d) The enhanced loss ability might arise from the efficient dielectric friction and interface resonates in the micro-scaled tetrapod-hollow structures. It can be expected that T-hollow with suitable electrical conductivity and micro-and/or nanoscale structures of cavities besides chirality from helix, plays a unique role in this kind of new structures.

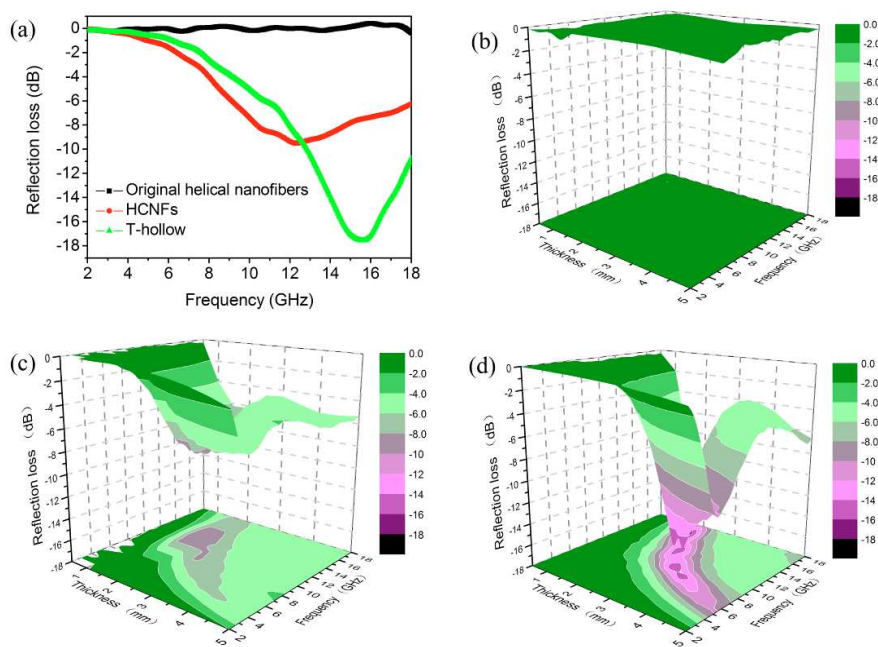


Fig. 8 (a) Microwave RL curves of the samples/wax composites with a thickness of 3 mm in the frequency range of 2–18 GHz, and simulated curves of electromagnetic wave loss of (b) original helical nanofiber, (c) carbon nanofiber and (d) helical fiber with tetrapod-hollow structure (namely T-hollow).

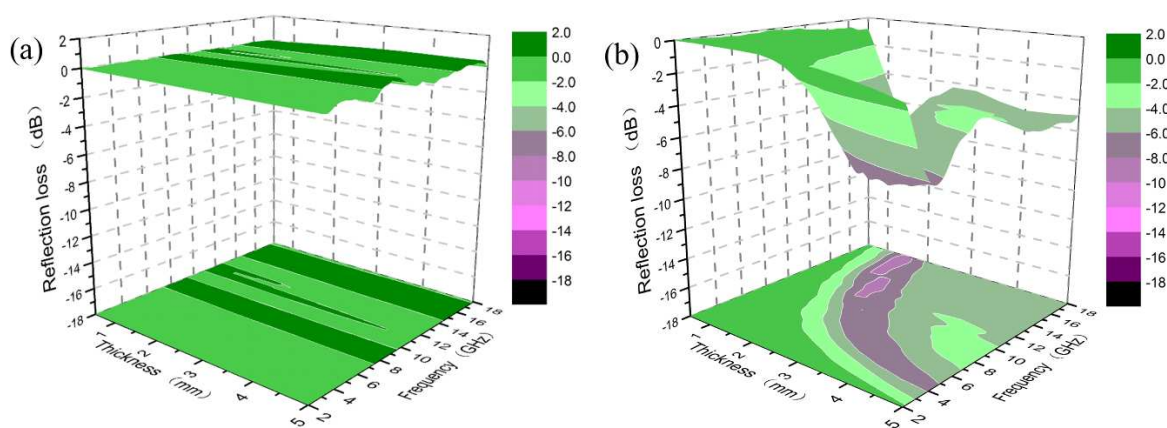


Fig. 9 Simulated curves of electromagnetic wave loss of straight original nanofibers and straight carbon fibers.

Experimental details

Materials

T-ZnO were obtained from oxidation reaction of metallic zinc by the gas expanding method as our earlier study.⁴¹ Metallic zinc in the forms of pellets or sheets (industrial-grade purity) was burned into T-ZnO particles at 500–800°C, keeping with the gate of the furnace was closed without special sealing during the whisker generation process. A white, fluffy product was obtained, with a yield of over 95% whiskers. All the chemicals including acetylene (C_2H_2), copper dichloride ($CuCl_2$) and potassium sodium tartrate ($C_4O_6H_4KNa$) were purchased from commercial sources with analytical grade and were used as received without further purification. All experiments were carried out using deionized water.

Preparation of helical fibers/T-ZnO and T-hollow carbon

The T-ZnO whiskers decorated with copper tartrate were prepared by the precipitation method using copper chloride and sodium potassium tartrate both at the concentration of 0.1 mol/L (M). The mole ratio of Cu to ZnO was adjusted in the range of 0.2–1.0 mol%. T-ZnO particles loaded Cu^{2+} ions after being immersed in $CuCl_2$ solution under magnetic stirring for 30 min. Then, $C_4H_4O_6KNa$ solution was dropped into T-ZnO suspension with stirring to form copper tartrate on the surface of T-ZnO. The obtained supported catalyst, namely copper tartrate/T-ZnO, was used for the growth of helical nanofibers according to our earlier reported gas-induced method under C_2H_2 at 271°C.²⁵ Firstly, copper tartrate decomposed into Cu nanocrystals. After that, the helical nanofibers were *in situ* synthesized around the T-ZnO whiskers using catalytic chemical vapor deposition (CCVD) method. The substrate decorated with copper tartrate was placed in the quartz tube of a chemical vapor deposition horizontal furnace. Ar and C_2H_2 gases were used for the exhaustion of Air in the tube and the synthesis of helical nanofibers, respectively. For the synthesis of high-purity helical nanofibers, C_2H_2 gas was introduced into the quartz tube at 271 °C and 60 mL/min for 60 min under the catalytic of gas-induced formation of copper nanocrystals keeping the setup closed without cooling. After heat-treatment under Ar at 900 °C, the HCNFs having tetrapod hollow (T-hollow) were prepared from the helical nanofibers/T-ZnO whiskers.

Characterization

Helical nanofibers/T-ZnO whiskers were characterized using a field emission scanning electron microscope (FE-SEM, Fei, Inspect-F) with an accelerating voltage of 20.0 kV and

transmission electron microscopy (Fei-F200) at an accelerating voltage of 200 kV, an X-ray diffraction spectrometer (XRD, Panalytical X'Pert PRO diffractometer with Ni-filtered, the Netherlands) and digital four-point probe system (SZ-82) at room temperature. For the evaluation of the microwave absorption properties of original helical nanofibers, helical nanofibers/T-ZnO and HCNFs with T-hollow, their mixture with paraffin were pressed into toroidal shaped samples of 7.0 mm outer diameter and 3.4 mm inner diameter, respectively. The electromagnetic parameters of the sample with 10 wt% helical materials were measured at 2–18 GHz with an AV3618 network analyzer. The reflection loss R (dB) of helical materials composites were calculated according to the transmit-line theory, using the measured data of relative complex permeability and permittivity.

Conclusions

In the frequency of 2–18 GHz, HCNFs had only dielectric loss and the reflection loss values were higher than -10 dB, while the original helical fibers exhibited neither dielectric loss nor magnetic loss due to the low electrical conductivity. Interestingly, HCNFs with T-hollow exhibited remarkably improvement in electromagnetic wave loss compared with the pure helical nanofibers. The enhanced loss ability might arise from an improved impedance match, the efficient dielectric friction and interface resonate in the complex nanostructures and the micro-scaled tetrapod-hollow structures. It can be expected that T-hollow with suitable electrical conductivity and micro-and/or nanoscale structures of cavities besides chirality from helix, plays a unique role in design of new functional materials.

Acknowledgements

This work was financially supported by the Open Foundation of State Key Laboratory of Electronic Thin Films and Integrated Devices(KFJJ201411), National Natural Science Foundation of China (No. 51173148, 51302230 and 51402040) the Special Research Fund for Doctoral Program of Higher Education (No. 20060613004), the NBRP (Grant No. 2011CB606200), and the Fundamental Research Funds for the Central Universities (No. 2010XS31 and No. SWJTU11ZT10). We would like to express our appreciation for the helpful comments of Dr. Yong Qin at Chinese Academy of Science and Dr. Weidong He at UESTC.

References

1. L. Zhang, J. Zhao, J. Zheng, L. Li and Z. Zhu, *Sensors and Actuators B: Chemical*, 2011, 158, 144-150.
2. S. Li, K. Yu, Y. Wang, Z. Zhang, C. Song, H. Yin, Q. Ren and Z. Zhu, *CrystEngComm*, 2013, 15, 1753-1761.
3. R. Paul, A. A. Voevodin, D. Zemlyanov, A. K. Roy and T. S. Fisher, *Adv Funct Mater*, 2012, 22, 3682-3690.
4. C. Yan, W. Xi, W. Si, J. Deng and O. G. Schmidt, *Adv Mater*, 2013, 25, 539-544.
5. G. Hu, F. Nitze, T. Sharifi, H. R. Barzegar and T. Wågberg, *J Mater Chem*, 2012, 22, 8541-8548.
6. C.-L. Zhu, M.-L. Zhang, Y.-J. Qiao, G. Xiao, F. Zhang and Y.-J. Chen, *J Phys Chem C*, 2010, 114, 16229-16235.
7. X. F. Zhang, X. L. Dong, H. Huang, Y. Y. Liu, W. N. Wang, X. G. Zhu, B. Lv, J. P. Lei and C. G. Lee, *Appl Phys Lett*, 2006, 89, 053115.
8. E. Martono, M. P. Hyman and J. M. Vohs, *Phys Chem Chem Phys*, 2011, 13, 9880-9886.
9. W. Cai, N. Homs and P. Ramirez de la Piscina, *Green Chem*, 2012, 14, 1035-1043.
10. X. Zhou, J. Qu, F. Xu, J. Hu, J. S. Foord, Z. Zeng, X. Hong and S. C. Edman Tsang, *Chem Commun*, 2013, 49, 1747-1749.
11. Q. Song, K.-z. Li, H.-l. Li, H.-j. Li and C. Ren, *Carbon*, 2012, 50, 3949-3952.
12. X. Ren, H. Zhang and Z. Cui, *Mater Res Bull*, 2007, 42, 2202-2210.
13. B. Adhikari, J. Nanda and A. Banerjee, *Soft Matter*, 2011, 7, 8913-8922.
14. E. Busserson, Y. Ruff, E. Moulin and N. Giuseppone, *Nanoscale*, 2013, 5, 7098-7140.
15. S. I. Stupp, R. H. Zha, L. C. Palmer, H. Cui and R. Bitton, *Faraday Discuss*, 2013, 166, 9-30.
16. D. Mandal, A. Nasrolahi Shirazi and K. Parang, *Organic & Biomolecular Chemistry*, 2014, DOI: 10.1039/C4OB00447G.
17. X. Qi, Q. Ding, W. Zhong, C.-T. Au and Y. Du, *Carbon*, 2013, 56, 383-385.
18. A. Shaikjee and N. J. Coville, *Journal of Advanced Research*, 2012, 3, 195-223.
19. F. Nitze, M. Mazurkiewicz, A. Malolepszy, A. Mikolajczuk, P. Kędzierzawski, C.-W. Tai, G. Hu, K. J. Kurzydłowski, L. Stobinski, A. Borodzinski and T. Wågberg, *Electrochim Acta*, 2012, 63, 323-328.
20. J. Zhou, J. He, G. Li, T. Wang, D. Sun, X. Ding, J. Zhao and S. Wu, *J Phys Chem C*, 2010, 114, 7611-7617.
21. H.-L. Xu, H. Bi and R.-B. Yang, *J Appl Phys*, 2012, 111, -.
22. P. Grünberg, D. E. Bürgler, H. Dassow, A. D. Rata and C. M. Schneider, *Acta Mater*, 2007, 55, 1171-1182.
23. Y. Qin, H. Li, Z. Zhang and Z. Cui, *Org Lett*, 2002, 4, 3123-3125.
24. X. Jian, M. Jiang, Z. Zhou, M. Yang, J. Lu, S. Hu, Y. Wang and D. Hui, *Carbon*, 2010, 48, 4535-4541.
25. X. Jian, M. Jiang, Z. Zhou, Q. Zeng, J. Lu, D. Wang, J. Zhu, J. Gou, Y. Wang, D. Hui and M. Yang, *ACS Nano*, 2012, 6, 8611-8619.
26. R. L. Schmid and J. Felsche, *Thermochim Acta*, 1982, 59, 105-114.
27. P. E. Laibinis and G. M. Whitesides, *J Am Chem Soc*, 1992, 114, 9022-9028.
28. M. Yang and J.-J. Zhu, *J Cryst Growth*, 2003, 256, 134-138.
29. S. Velu, K. Suzuki, C. S. Gopinath, H. Yoshida and T. Hattori, *Phys Chem Chem Phys*, 2002, 4, 1990-1999.
30. N. Pasha, N. Lingaiah, P. S. Reddy and P. S. S. Prasad, *Catal Lett*, 2009, 127, 101-106.
31. L. Jing, Z. Xu, X. Sun, J. Shang and W. Cai, *Appl Surf Sci*, 2001, 180, 308-314.
32. H. Zhang, X. Ren and Z. Cui, *J Cryst Growth*, 2007, 304, 206-210.
33. N. Tang, J. Wen, Y. Zhang, F. Liu, K. Lin and Y. Du, *ACS Nano*, 2010, 4, 241-250.
34. F. Nitze, E. Abou-Hamad and T. Wågberg, *Carbon*, 2011, 49, 1101-1107.
35. G. Wang, G. Ran, G. Wan, P. Yang, Z. Gao, S. Lin, C. Fu and Y. Qin, *ACS Nano*, 2014.
36. X. Zhang and S. K. Manohar, *Chem Commun*, 2006, 42, 2477-2479.
37. X. F. Zhang, H. Huang and X. L. Dong, *J Phys Chem C*, 2013, 117, 8563-8569.
38. G. Wang, Z. Gao, S. Tang, C. Chen, F. Duan, S. Zhao, S. Lin, Y. Feng, L. Zhou and Y. Qin, *ACS Nano*, 2012, 6, 11009-11017.
39. L. Liu, P. He, K. Zhou and T. Chen, *AIP Advances*, 2013, 3, -.
40. T. Zhao, C. Hou, H. Zhang, R. Zhu, S. She, J. Wang, T. Li, Z. Liu and B. Wei, *Sci. Rep.*, 2014, 4.
41. Z. Zhou, H. Deng, J. Yi and S. Liu, *Mater Res Bull*, 1999, 34, 1563-1567.